J Mol Model (2011) 17:2825–2830
DOI 10.1007/s00894-011-0972-0

ORIGINAL PAPER

Graphene-based pressure nano-sensors

Viacheslav Sorkin · Yong Wei Zhang

Received: 10 November 2010 / Accepted: 11 January 2011 / Published online: 2 February 2011

Abstract We perform atomistic simulations to study the failure behavior of graphene-based pressure sensor, which is made of a graphene nanoflake suspended over a well in a silicon-carbide substrate and clamped on its surrounding edge by the covalent bonds between the graphene flake and the substrate. Two distinct types of mechanical failure are identified: the first one is characterized by complete detachment of the graphene nanoflake from the silicon-carbide substrate via breaking the covalent bonds between the carbon atoms of the graphene flake and the silicon atoms of the substrate; the second type is characterized by the rupture of the graphene nanoflake via breaking the carbon-carbon bonds within the graphene. The type of mechanical failure is determined by the clamped area between the graphene flake and the substrate. The failure pressure can be tuned by changing the clamped area and the well radius. A model is proposed to explain the transition between the two types of failure mode. The present work provides a quantitative framework for the design of graphene-based pressure sensors.

Keywords Graphene · Graphene-based pressure detector · Failure mechanism · Nanosensor · Silicon carbide · Single-use (disposable) technology

PACS 81.05.Uw · 71.15.Mb · 68.37.Ef

V. Sorkin (✉) · Y. W. Zhang
Institute of High Performance Computing,
Singapore 138632, Singapore
e-mail: sorkinv@ihpc.a-star.edu.sg

Introduction

Sensors are always in great demand in scientific and industrial applications, and a search for new materials in sensor applications persists at all times. Emerging nano-technologies promise to create the next generation of sensors, exploiting novel properties and phenomena occuring on the nano scale. Nanosensors are expected to have substantially smaller size and lower weight, leading to higher sensitivity, better specificity and exceptional stability. The discovery of carbon nano-tubes [1–5], and graphene [6, 7] has generated great interest to develop these nanosensors [8–11].

The development of one class of nanosensors - pressure nanosensors - based on graphene is a promising line of research. Pressure nanosensors can be designed by taking advantage of the unique electro-mechanical properties of graphene. However, in order to design the nanosensors, we need to understand the electric and mechanical properties of graphene. We also need to understand the interaction between graphene and other building blocks in the nano-sensors. So far, many interesting results have been obtained in these areas. For example, the mechanical response of graphene to an external load was studied by indentation experiments and by computer simulations [12]. Bunch et al. [13] created a prototype for pressure sensor by placing a graphene flake over a well in silicon dioxide. Permeability of graphene was investigated by applying pressure difference across the graphene sheet. It was found that graphene is impermeable to standard gases, and concluded that it can be used as a highly sensitive pressure sensor [13]. Schedin et al. [14] found that even a small local strain of graphene induced by a single adsorbed molecule is detectable [14, 15]. Furthermore, they experimentally detected local changes in electrical resistance around a single molecule adsorbed on graphene, and measured the induced strain.

The prototype of sensor proposed in Bunch et al. [13] was based on the van der Waals force between the graphene flake and the silicon dioxide substrate. Since the van der Waals interaction is rather weak, the detection of pressure is expected to operate in a low-pressure regime. It has been shown that graphene flake and silicon carbide substrate form covalent bonds between the carbon atoms of the graphene flake and the silicon atoms of the silicon carbide surface [16, 17]. Since the covalent bonding between the graphene flake and the silicon carbide surface is strong, the graphene flake-silicon carbide-based sensor is expected to work in a high pressure regime and have much better sealing ability. Therefore, it is important to investigate the mechanical properties and failure behavior of such graphene based pressure sensors.

In the present work, we constructed a simple atomistic model for graphene nanoflakesilicon carbide-based pressure nanosensor. Using this model we studied the failure behavior of the sensor under an applied pressure. Two different mechanisms of failure were identified and discussed. The present work on the mechanical behavior of the graphene-silicon carbide-based sensor potentially provides useful information for the design and fabrication of such sensors.

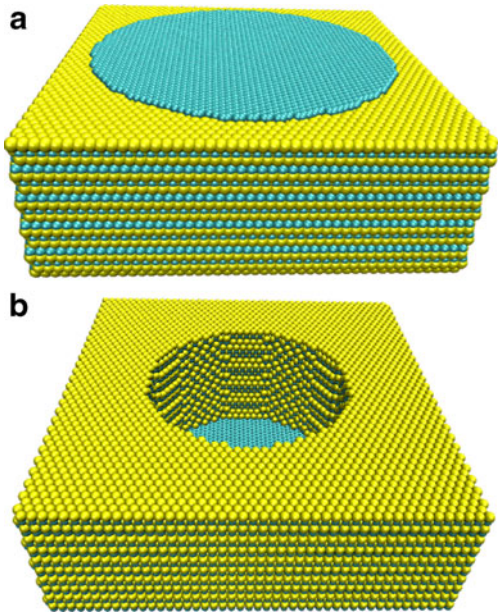

Fig. 1 (Color online) Sample schematic: the Si-terminated 6H-SiC (0001) substrate with a cylindrical well covered by a graphene nanoflake. Silicon atoms are marked in yellow and carbon atoms in blue. (**a**) Top view. (**b**) Bottom view

Computational model

In our model, we constructed a 6H-SiC allotrope of silicon carbide with the Si-terminated SiC(0001) surface. The silicon carbide substrate consisted of 16 carbon-silicon bilayers. The two SiC bilayers at the bottom of the substrate were fixed to mimic a semi-infinite substrate. Periodic boundary conditions were applied along the X and the Y directions.

To model the graphene-based pressure sensor, a cylindrical well was cut in the siliconcarbide substrate (see Fig. 1). A circular graphene nanoflake was placed on the substrate surface to seal the cylindrical well opening. Hence, the inner part of the graphene nanoflake was suspended while the outer part of the graphene nanoflake was supported by the underlying substrate. Subsequently, an external force along the out-of-plane direction (perpendicular to the surface) was applied to each atom of the graphene nanoflake and the surface of the substrate to mimic the application of pressure. The external force (load) is the total applied force calculated as a sum over all graphene atoms. This definition is used throughout our manuscript.

In our simulations, we varied the width of the suspended part of the graphene nanoflake and the radius of the cylindrical well to examine the failure behavior of the sensor. The radius of the cylindrical well, R, was varied between $R = 10.0\mathring{A}$ and $R = 50.0\mathring{A}$. The width of the supported part of the graphene nanoflake, W, was changed from $W = 2.0\mathring{A}$ to $W = 30.0\mathring{A}$. The substrate size was adapted to the dimensions of the radius and width of the graphene nanoflake. The number of graphene atoms used in our simulations ranged from N=5852 for the smallest graphene flake to N=119260 for the largest one. The initial distance between the graphene nanoflake and the substrate was set to $Z = 2.3\mathring{A}$. This distance was chosen to provide the fastest convergence for the total energy minimization using the conjugate gradient method.

We applied a semi-empirical many-body potential introduced by Tersoff [18] to describe the C-C, C-Si and Si-Si inter-atomic interactions. This potential was recently successfully employed to study silicon carbide [19], graphene supported on silicon carbide [16, 17], carbon nano-tubes [20, 21], silicon nano-tubes [22] and fullerenes [23]. The conjugate gradient method was applied in our simulations to minimize the total energy of our samples. Total energy minimization was performed at zero temperature. Subsequently we investigated the morphology of a graphene flake as a function of the applied load and identified the mechanism of failure of the pressure sensor. The conjugate gradient method applied in our simulation was implemented as part of the large-scale atomic/molecular massively parallel simulator (LAMMPS) code [24].

Results and discussion

First, we placed a circular graphene nanoflake on the top of the Si-terminated 6HSiC(0001) substrate surface to seal the

cylindrical well and then minimized the total energy of the system. Analysis of the obtained minimal energy configuration shows that covalent Si-C bonds are formed at the graphene nanoflake-substrate interface. These Si-C bonds literally clamped the graphene flake on the substrate surface. Due to the bond formation, ripples emerged in the part of the graphene nanoflake supported by the substrate. The ripple formation is due to the combined effect of the van der Waals interaction and bond formation between the graphene nanoflake and the substrate. The properties of these ripples were thoroughly investigated in our earlier work [16, 17].

After the initial relaxation of the system, an external normal force was applied to each atom of the nanoflake and the top surface layer to mimic the external pressure. At each step, the applied force was gradually increased and the total energy was minimized.

Initially, when the applied load was moderate, the Si-C covalent bonds were strained (see Fig. 2a), but not broken. The bond deformation was elastic and reversible. As we proceeded to increase the external load, the graphene flake began to deflect further down and acquired a lens shape. When the external load was increased further, we observed two types of failure mode depending on the width of the supported region.

When the area of the supported region was small, for example, a graphene flake with the radius of 50$\AA$ and the supported part width of 20$\AA$, a few radially-oriented wrinkles appeared at the supported region of the graphene flake (see Fig. 2c). The average height of these wrinkles was about 5$\AA$. The wrinkles extended down to the suspended part of the graphene flake. The characteristic penetration length of the deformation was about 12$\AA$. The wrinkle formation was accompanied by irreversible Si-C bond breaking at the nanoflake-substrate interface as shown in Fig. 2 (see the upper panel: b-c). The number of the established Si-C bonds was noticeably decreased. When the load increased to a critical value, mechanical failure through interface delamination between the graphene and substrate occurred. As a result, the graphene nanoflake was detached from the substrate and forced down into the well (see Fig. 3) in the substrate. In the subsequent discussion, we refer to this failure mechanism as delamination, which takes place when the clamped graphene region on the substrate is narrow.

If the width of this graphene clamped region was increased, the critical load for delamination was also increased. However, when the width of this region was increased to a critical value, a transition of failure mode was observed, where the graphene fracture occurred instead of interface delamination. For example, when a graphene nanoflake with a radius of $R = 30\AA$ and a width of the supported region $W = 24\AA$ was used, a small narrow crack appeared at the boundary between the suspended and clamped part of the graphene flake (see Fig. 4). This crack advanced rapidly until the suspended part of the graphene

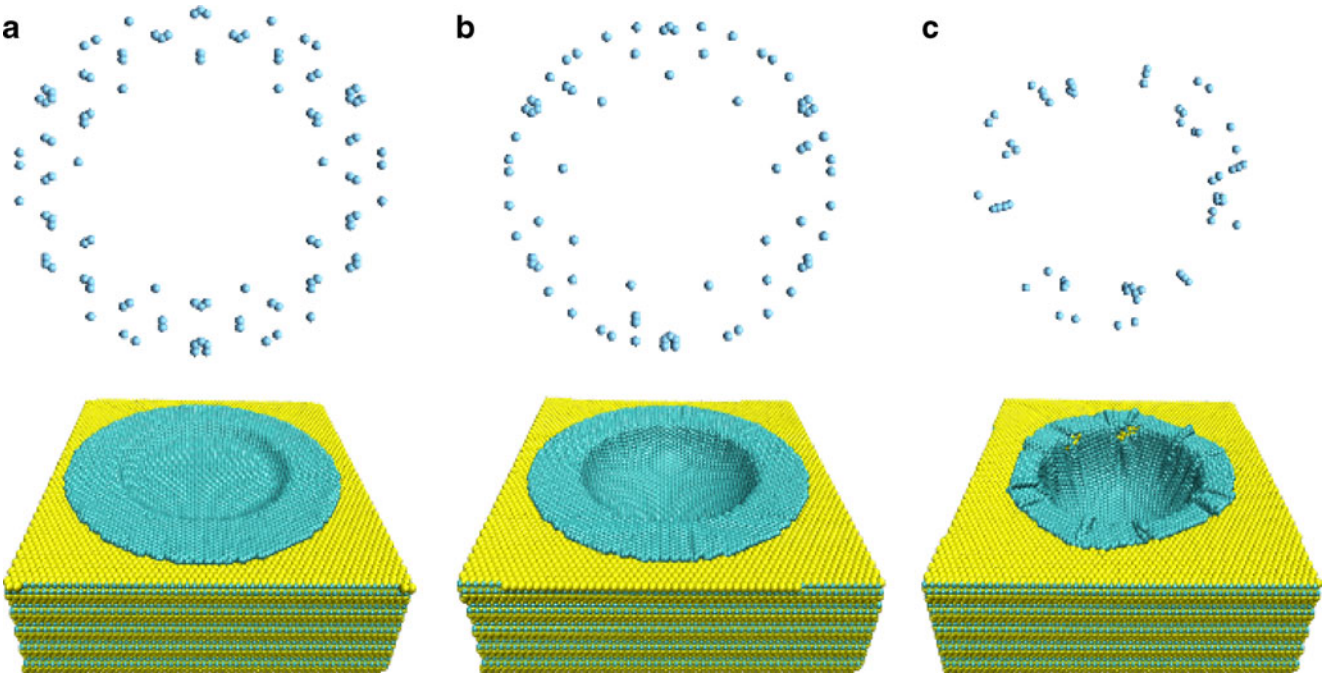

Fig. 2 (Color online) Graphene nanoflake supported by the Si-terminated SiC(0001) substrate is subjected to an external load. Top panel: distribution of the Si-C bonds at the nanoflake-substrate interface. Bottom panel: shape of the graphene nanoflake under the effect of the external load, f: (**a**) f=0.24 μN, (**b**) f=0.72 μN, and (**c**) f= 0.98 μN. The radius of the graphene nanoflake is $R = 50\AA$ and the width of its region accommodated on the substrate is $W = 20\AA$.

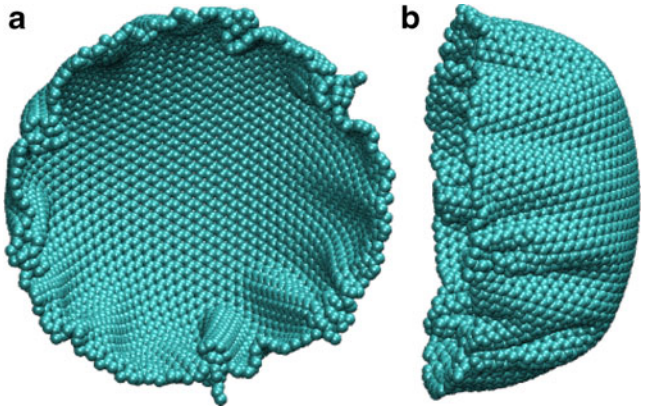

Fig. 3 (Color online) Graphene nanoflake with radius $R = 40\dot{A}$ under the effect of an external load of f=0.56 μN Width of the supported region is $W = 20\dot{A}$. (**a**) Top view. (**b**) Side view

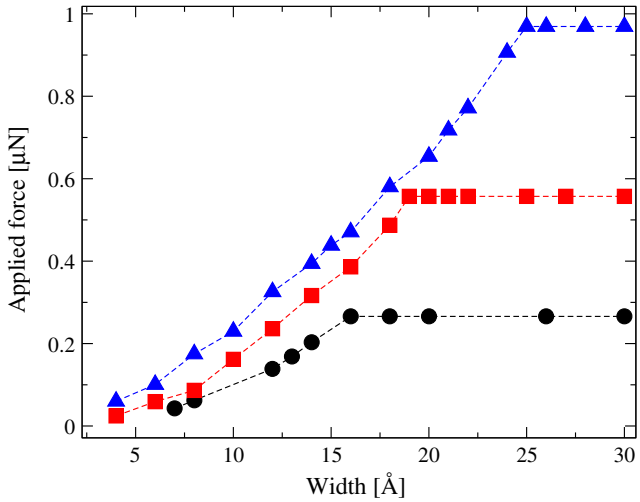

Fig. 5 Critical applied force causing mechanical failure of a graphene flake as a function of the clamping width. The radius of the internal part of the graphene flake is R = $10\dot{A}$ (circles), R = $30\dot{A}$ (squares) and R = $50\dot{A}$ (triangles)

flake was torn apart. As a result, only a few remnants of the flake remained on the substrate.

The crossover point between these two different mechanisms of failure can be identified in Fig. 5, where we have plotted the critical force causing the mechanical failure of the graphene flake as a function of the clamping width. As it is shown in Fig. 5, the critical force for interface delamination initially increases super-linearly with the clamping width. However, when the width of this region reaches a critical value, the external force causing the failure of the graphene flake is no longer dependent on the clamping width. This clamping width independent regime corresponds to the failure mechanism due to graphene fracture.

In order to explain the transition of the failure mode, we have calculated the critical forces (per unit length) required to delaminate the nanoflake from the substrate and to fracture the graphene membrane, respectively. Our simulations show that the critical force required to delaminate the nanoflake from the substrate increases with the width of the clamped region. When the width of the clamped region of the graphene flake is sufficiently large, the critical load for the delmaination failure should become independent of its width, which corresponds to the upper bound for interface delamination. If this upper bound critical load is larger than the critical load for graphene fracture, a transition of failure from inteface delamination to graphene fracture should occur. Otherwise, there should be no transition in the failure mode.

The upper bound critical load can be estimated using the energy balance theory of fracture applied to thin-film peeling [25]. In this case, the upper bound critical delamination force per unit length is given by:

$$f_d = \sqrt{2E_p\gamma}, \tag{1}$$

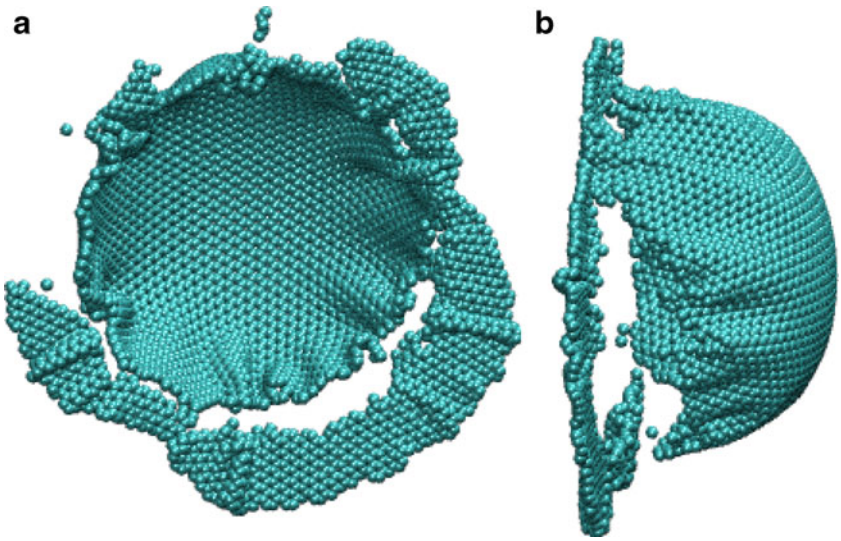

Fig. 4 (Color online) Graphene nanoflake with radius $R = 30\dot{A}$ under the effect of an external load of f=0.58 μN Width of the supported region is $W = 24\dot{A}$. (**a**) Top view. (**b**) Side view

where E_p is the in-plane elastic modulus of graphene and γ is the interfacial energy between the graphene and the SiC substrate. The value of $E_p = 20eV/\AA^2$ was calculated in [26] and $\gamma \simeq 0.18eV/\AA^2$ is obtained using:

$$\gamma = \frac{E_{tot} - E_{gr} - E_{SiC}}{A}, \quad (2)$$

where A is the area of the graphene nanoflake, E_{gr} is its energy, E_{SiC} is the energy of the silicon-carbide substrate and E_{tot} is the energy of the graphene nanoflake supported by the substrate. Using these values, we found that the upper bound for the critical force per unit length is $f_d \simeq 43\text{N/m}$.

The breaking strength of graphene membrane can be estimated using our atomistic simulation data in Fig. 5. Since the graphene nanoflake fractures at the edge of the cylindrical well with the radius R, we estimated the breaking strength of graphene as $F_f/2\pi R$ (we approximate the length of the crack front as $2\pi R$). Using our simulation data (Fig. 5) to obtain F_f for various radii, we found that the breaking strengths are all about $\simeq 32\text{N/m}$, which is smaller than the upper bound critical delamination force per unit length, $f_d \simeq 43\text{N/m}$.

Since the graphene breaking strength is smaller than the upper bound delamination critical force per unit length, this explains the transition from the preceding interface delamination failure mechanism to the graphene fracture failure mechanism.

We note, however, that our estimated graphene breaking strength is well below the experimentally measured 42 N/m [27]. In the experiment, the breaking strength was measured for a free-standing graphene mono-layer under a uniform deformation (uniaxial strain). In our case, the graphene membrane was not in a uniformly stretched state, but sharply bent at the edge of the well. We argue that the discrepancy between our results and the experiment data, can be resolved when the effect of the sharp bending on the breaking strength of graphene is considered. In order to prove this, we calculated the breaking strength of a graphene ribbon bending over a corner of a SiC substrate by an external pulling force (see Fig. 6). We found that the breaking strength of graphene decreases nearly linearly with increasing the inclination angle (see Fig. 7). It is seen in Fig. 7 that for the stretching of a free standing graphene, the breaking strength is around 48 N/m, which is in agreement with the experimental measurements. When the inclination angle increases to 80°, the breaking strength reduces to about 32 N/m, which is in excellent agreement with our atomistic simulation result obtained above. Hence, the reduction of the breaking strength of graphene in the sensor is due to to lattice distortion arising from the graphene bending at the edge of the well. The bending distortion makes the C-C bonds weaker in the strained state, thus reducing the breaking strength.

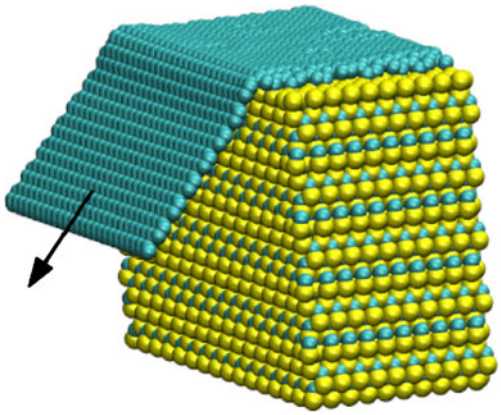

Fig. 6 External force applied to a graphene nanoribbon accommodated on the SiC substrate. Inclination angle of the applied force is 50°

Based on the above analysis of the failure mechanisms of the graphene nanoflake accommodated on the SiC substrate, we propose to construct a pressure detector. This pressure detector can be realized using an array of sensors, each one consisting of a graphene nanoflake sealing a well in the Si-terminated SiC(0001) substrate. The graphene nanoflakes for each sensor can be of different radii, but have the same width for the supported part. Alternatively, they can differ in the width of the supported part, but have the same radius. In either case, with the knowledge of the failure mechanisms, the failure pressure for each sensor can be predetermined. Hence, at certain external pressure, some sensor fails. Since the specifications of the failed sensor, such as the radius of the suspended part and the width of clamped part of graphene flake are known, the applied pressure can be inferred by using the obtained relation between the sensor geometry and the failure characteristics (see Fig. 5).

The proposed nano-sensors can be used to measure pressure in the range between 10 and 80 GPa. This pressure

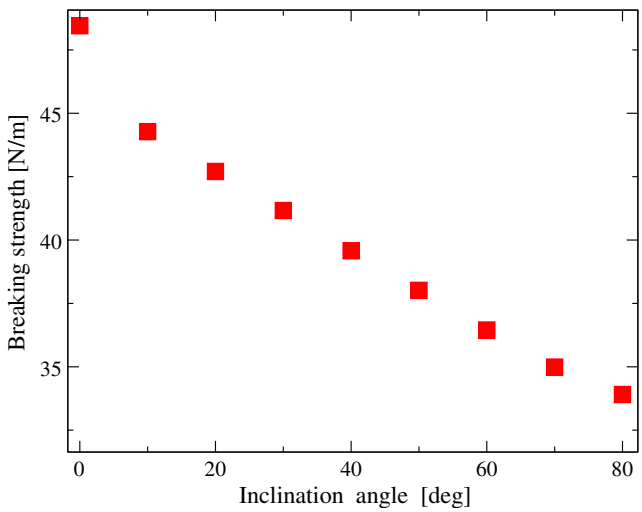

Fig. 7 Breaking strength of graphene nanoribbon as a function of the inclination angle at which force is applied

range is estimated using the calculated limits of the applied critical force, divided by the sensor area. In this pressure arrange, the proposed sensors may have many potential applications, especially when local allowable high peak pressure is needed to be precisely monitored. For example, our proposed graphene based single-use pressure sensors can find their applications in alarm systems to notify the user of pressure exceeding a specified threshold.

The operational concept of the proposed pressure sensor is based on the failure mechanism of graphene on the (0001) SiC substrate. Thus the proposed sensor is a single-use (dispos-able) one. In many industrial applications, single-use sensors, which are often cost-effective in manufacturing and easy to use in operations, have provided a practical alternative to reusable ones. So far, they have been widely used not only in biomedical and pharmaceutical applications, but also in some traditional areas, such as hazardous materials processing, where single-use technology offers additional protection [28].

Conclusions

We studied the mechanical failure of pressure sensors based on graphene nanoflake using atomistic approach. The pressure sensor consisted of a circular graphene nanoflake sealing a cylindrical well in an underlying silicon-carbide substrate. The failure behavior of the sensor subjected to an external load was investigated using a semi-empirical many-body potential introduced by Tersoff [18].

It was found that the initial flat shape of the suspended graphene nanoflake was deflected by the applied load. When the applied load reached a critical value, the graphene sensor failed. Two distinct types of mechanical failure were identified. The first type was characterized by a complete detachment of the graphene flake from the supporting substrate. The second type was characterized by the fracture of atomic bonds within the graphene flake. The width of the clamped region of the graphene flake (attached to the underlying substrate) determined which type of mechanical failure occurred. If the width was smaller than a critical value, the sensor failed due to graphene detachment (the first type mechanism). If the width was above the critical value, the sensor failed due to graphene fracture (the second type mechanism). The critical value of the width depends on the radius of the graphene nanoflake. The present investigation provides useful information for the potential application of graphene nanoflakes in nanoelectromechanical systems.

Acknowledgments This work was funded by the Agency for Science, Research and Technology (A*STAR), Singapore. Graphic images were made with the Visual Molecular Dynamics (VMD) visualization package [29]. The Large-scale Atomic/Molecular Massively Parallel Simulator (LAMMPS) [24] code used in our simulations was distributed by Sandia National Laboratories.

References

1. Dai H (2002) Sur Sci 500:218
2. Dresselhaus M, Dai H (2004) MRS Bull 29:237
3. Harris PJF, Hernndez E, Yakobson BI (2004) Am J Phys 72:415
4. Thostensona ET, Renb Z, Chou T-W (2001) Compos Sci Technol 61:1899
5. Treacy MMJ, Ebbesen TW, Gibson JM (1996) Nature 381:678
6. Meyer JC, Geim AK, Katsnelson MI, Novoselov KS, Booth TJ, Roth S (2007) Nature 446:63
7. Novoselov KS, Geim AK, Morozov SV, Jiang D, Zhang Y, Dubonos SV, Grigorieva IV, Firsov AA (2004) Science 306:666
8. Hierold C (2004) J Micromech Microeng 14:S1
9. Lia C, Thostensona ET, Cho T-W (2008) Compos Sci Technol 68:1227
10. Roman C, Helbling T, Hierold C (2010) Single-walled carbon nanotube sensor concepts. Springer, Berlin
11. Sinha N, Ma J, Jeow JTW (2006) J Nanosci Nanotechnol 6:573
12. Wang CY, Mylvaganam K, Zhang LC (2009) Phys Rev B 80:155445
13. Bunch JS, Verbridge SS, Alden JS, van der Zande AM, Parpia JM, Craighead HG, McEuen PL (2008) Nano Lett 8:2458
14. Schedin F, Geim AK, Morozov SV, Hill EW, Blake P, Katsnelson MI, Novoselov KS (2007) Nat Mater 6:652
15. Rangel NL, Seminario JM (2008) J Phys Chem A 112:13699
16. Sorkin V, Zhang YW (2010) Phys Rev B 81:085435
17. Sorkin V, Zhang YW (2010) Phys Rev B 82:085434
18. Tersoff J (1989) Phys Rev B 39:5566
19. Ivashchenko VI, Turchi PEA, Shevchenko VI, Shramko OA (2004) Phys Rev B 70:115201
20. Lopez MJ, Cabria I, March NH, Alonso JA (2005) Carbon 43:1371
21. Zang J, Treibergs A, Han Y, Liu F (2004) Phys Rev Lett 92:105501
22. Won KJ, Jeong SJ, Jung HH (2002) J Nanosci Nanotechnol 2:687
23. Halac EB, Reinoso M, Dall'Asen AG, Burgos E (2005) Phys Rev B 71:115431
24. Plimpton SJ (1995) J Comp Phys 117:1
25. Kendall K (1975) J Phys D Appl Phys 8:1449
26. Shenoy VB, Reddy CD, Ramasubramaniam A, Zhang YW (2008) Phys Rev Lett 101:245501
27. Lee C, Wei X, Kysar JW, Hone J (2008) Science 321:385
28. Sandstrom C (2009) Chem Eng Prog 105:30
29. Humphrey W, Dalke A, Schulten K (1996) J Mol Graph 14:33